Article

Study of DNA Interaction and Cytotoxicity Activity of Oxidovanadium(V) Complexes with ONO Donor Schiff Base Ligands

Gurunath Sahu [1], **Edward R. T. Tiekink** [2] and **Rupam Dinda** [1,*]

[1]   Department of Chemistry, National Institute of Technology, Rourkela, Odisha 769008, India; 518cy1003@nitrkl.ac.in

[2]   Research Centre for Crystalline Materials, School of Medical and Life Sciences, Sunway University, Bandar Sunway 47500, Selangor Darul Ehsan, Malaysia; edwardt@sunway.edu.my

*   Correspondence: rupamdinda@nitrkl.ac.in

Abstract: Two new oxidovanadium(V) complexes, $(HNEt_3)[V^VO_2L]$ (**1**) and $[(V^VOL)_2\mu\text{-}O]$ (**2**), have been synthesized using a tridentate Schiff base ligand H_2L [where H_2L = 4-((E)-(2-hydroxy-5-nitrophenylimino)methyl)benzene-1,3-diol] and $VO(acac)_2$ as starting metal precursor. The ligand and corresponding metal complexes are characterized by physicochemical (elemental analysis), spectroscopic (FT-IR, UV–Vis, and NMR), and spectrometric (ESI–MS) methods. X-ray crystallographic analysis indicates the anion in salt **1** features a distorted square-pyramidal geometry for the vanadium(V) center defined by imine-N, two phenoxide-O, and two oxido-O atoms. The interaction of the compounds with CT–DNA was studied through UV–Vis absorption titration and circular dichroism methods. The results indicated that complexes showed enhanced binding affinity towards DNA compared to the ligand molecule. Finally, the in vitro cytotoxicity studies of H_2L, **1**, and **2** were evaluated against colon cancer (HT-29) and mouse embryonic fibroblast (NIH-3T3) cell lines by MTT assay. The results demonstrated that the compounds manifested a cytotoxic potential comparable with clinically referred drugs and caused cell death by apoptosis.

Keywords: Oxidovanadium(V); Schiff base; X-ray crystallography; DNA interaction; cytotoxicity

1. Introduction

In the family of the vanadium complexes, the oxoidovanadium Schiff base complexes are the most rapidly growing class owing to their rich underlying features and vital role during the process of interaction with various biomolecules [1]. Although vanadium exists in different oxidation states from −III to +V, for the higher oxidation states (+IV and +V), vanadium is highly stable and can form oxophilic complexes [2–4]. Oxidovanadium complexes have various roles in biochemical processes, such as nitrogen fixation, haloperoxidation, and glycogen metabolism [5,6]. In recent years, the investigation of the antifungal, antibacterial, and anticancer activities of these complexes has become the main subject of many studies. Recently, there is a growing interest in the in vitro and in vivo studies of vanadium complexes towards the treatments of diabetes and cancer [7,8]. After the discovery of many oxidovanadium drugs, bis(maltolato)oxovanadium(IV), BMOV, as glucose and lipid-lowering insulin mimetics, the focus on these types of compounds was stimulated [9]. Additionally, the anticancer activity of vanadium complexes has been widely examined on trial carcinogenesis and tumor-bearing animals [10,11]. The anticancer activity of several oxidovanadium complexes has recently received attention due to physiochemical changes in the solution medium leading to reduced systemic toxicity with beneficial effects [12,13]. There are also reports that vanadium accumulates in cancerous cells and tissues more than in normal cells [11,14]. For this reason, vanadium complexes have displayed promising cytotoxicity against various human cancer cell lines and these complexes were found to show

better selectivity and higher cytotoxicity with reduced side effects. Therefore, attempts are being made to develop anticancer drugs using these oxidovanadium(V) complexes as suitable alternatives to platinum-based drugs [15].

In addition, Schiff bases play an immense role in coordination chemistry due to their ability to stabilize metal ions in various oxidation states, and their participation in numerous catalytic applications and biological activities [16–18]. The formation of stable metal complexes is due to the nitrogen lone pair of electrons present in the azomethine (−N=CH) backbone of the ligand molecule [18,19]. Various types of Schiff base ligands have been explored for their fascinating and significant properties, for example, complexing ability towards a wide range of transition metals, and applications in biological activity [20,21]. Certain oxidovanadium(V) Schiff base complexes have been reported earlier as model compounds, displaying biomolecular interactions with proteins and bio-ligands such as DNA [8,22,23]. Additionally, it is demonstrated that with increase in substitution and planarity of ligands, DNA interactions are enhanced [24]. Furthermore, metal complexes which can effectively interact with DNA under physiological conditions are considered to be possible contenders for use as therapeutic agents in medicinal applications and for genomic research [24,25]. Therefore, attempts are being made to develop anticancer drugs using these oxidovanadium(V) complexes as suitable alternatives to platinum-based drugs. Reportedly, polyphenolic/polyhydroxy compounds can prevent oxidative damage as they can scavenge reactive oxygen species such as hydroxyl radicals and superoxide anions. The prooxidant properties of polyphenolic compounds may contribute to tumor cell apoptosis [26–28]. In consideration of the inherent property of phenols and other polyhydroxy compounds particularly for medicinal and pharmacological applications [29,30], their corresponding complexes might be crucial for investigation for anticancer activity.

In continuation of our previous work on the synthesis, characterization, and biological studies of vanadium(V/IV) complexes [8,13,31–45], here we report a new mononuclear dioxidovanadium(V) (**1**) as well as an oxido-bridged dinuclear oxidovanadium(V) (**2**) complex, each with a tridentate ONO donor Schiff base ligand derived from 2,4-dihydroxybenzaldehyde and 2-amino-4-nitrophenol. Considering the therapeutic potential of the synthesized polyphenolic ligand molecule [27,30,46], corresponding oxidovanadium(V) complexes were synthesized to further investigate their pharmacological activities such as DNA interaction and anticancer activities. The primary objective of this current work was to investigate the significant characteristics of these ligand(H_2L) and oxidovanadium(V) complexes in terms of their applications as anticancer agents. The synthesized ligand and respective complexes were characterized by various spectroscopic (FT-IR, UV–Vis, and NMR), spectrometric (ESI–MS) techniques and the purity of the compounds were confirmed by CHN analysis. Furthermore, the single-crystal X-ray crystal structure of **1** was determined. The binding of the complexes toward CT–DNA was studied by UV–Vis absorption titration and circular dichroism. Finally, the cytotoxicity of the synthesized compounds was determined against HT-29 cell lines by MTT assay and for comparison a normal cell line, mouse embryonic fibroblast (NIH-3T3), was used.

2. Results and Discussion

2.1. Synthesis

New mononuclear dioxidovanadium(V) (**1**) and oxido-bridged dinuclear oxidovanadium(V) (**2**) complexes were synthesized by the reaction of the metal precursor $[V^{IV}O(acac)_2]$ with a tridentate ONO donor Schiff base ligand (H_2L) derived from condensation of 2,4-dihydroxybenzaldehyde and 2-amino-4-nitrophenol under reflux conditions. Scheme 1 depicts the synthetic methods of preparation of the complexes. The compounds were characterized by several spectroscopic (FT-IR, UV–Vis, and NMR) and spectrometric (ESI–MS) methods, and their purity was further confirmed by CHN elemental analysis. The structure of **1** was determined by single-crystal X-ray crystallography.
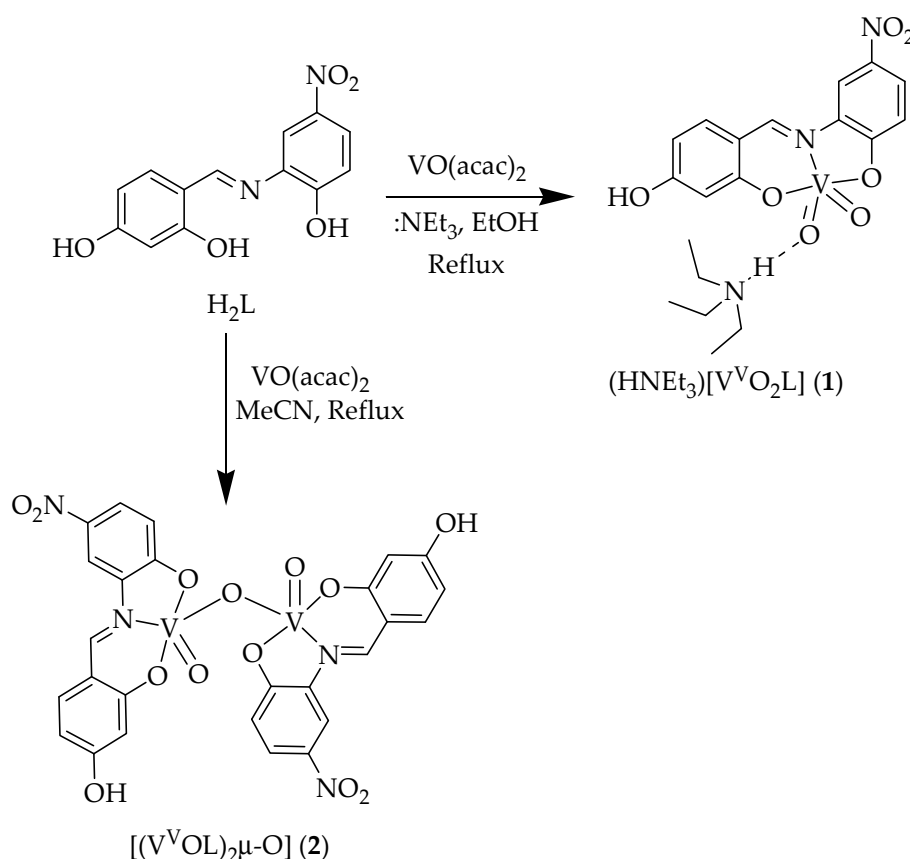
Scheme 1. Outline of the pathways for the synthesis of (HNEt$_3$)[V^{V}O$_2$L] (**1**) and [(V^{V}OL)$_2$μ-O] (**2**).

2.2. Spectral Characteristics

2.2.1. IR Spectroscopy

Selected spectroscopic data of ligand (H$_2$L) and respective complexes (**1** and **2**) have been compiled in the Experimental Section. The IR spectrum of the free ligand (H$_2$L) exhibits one sharp band in the region 3205 cm^{-1} due to ν(O–H) stretching vibrations, which is absent in the corresponding metal complexes due to deprotonation of phenolic hydrogen [40]. Furthermore, the stretching band found in the region 1632–1607 cm^{-1} clearly indicates the presence of ν(C=N) in the ligand as well in the complexes [38]. In addition, two additional new stretching bands appeared in the region 888 and 947 cm^{-1} assigned to the two ν(V=O) stretching of cis-ν(V=O) groups in **1** whereas for **2** it is observed in the region 891 and 975 cm^{-1}. These stretching vibrations are in agreement with the terminal V=O groups present in related oxidovanadium(V) complexes [43]. Additionally, a new stretching band observed at 819 cm^{-1} assigned to the ν(V–O–V) residue of complex **2** which further indicates the existence of a dinuclear species [45]. The representative IR spectra of the ligand (H$_2$L) and its corresponding complex **1** are depicted in Figure S1.

2.2.2. Electronic Spectra

The UV-visible spectra of the ligand (H$_2$L) and its complexes (**1** and **2**) were recorded in DMSO with a complex concentration of 1.6×10^{-4} M (Figure 1). The spectrum of the free ligand shows two strong absorptions in the region 317 and 278 nm whereas their respective complexes show three strong absorption bands in the region 446–264 nm. The low energy absorption bands observed for the complexes in the region 422 and 446 nm could be attributed to ligand to metal charge transfer (LMCT) transition whereas the high energy bands appeared in the UV region (361–264 nm) are likely to be due to ligand center transitions [34].

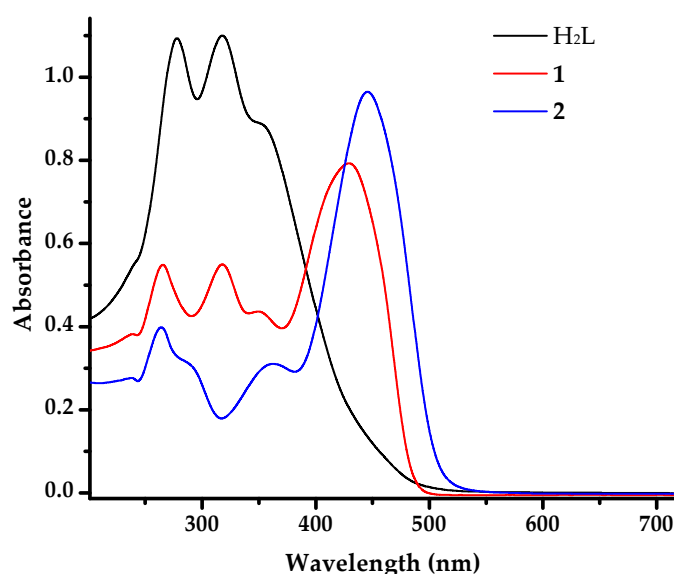**Figure 1.** UV–Vis spectra of H_2L, **1**, and **2** (1.6×10^{-4} M) in DMSO.

2.2.3. NMR Spectra

The ^{1}H and ^{13}C{^{1}H} NMR data of ligand was recorded in DMSO-d_6. The spectrum of H_2L exhibits two compounds connected via intermolecular hydrogen bonding as shown in Figure S2 due to which two equivalent sets of protons obtained in the NMR. The ^{1}H NMR spectra of H_2L show singlet resonances in the downfield region in the range δ = 10.92–8.95, and 8.21 ppm due to –OH, and –CH (azomethine) protons, respectively [42]. The aromatic protons were observed in the expected range between δ = 8.20-6.27 ppm [37]. However, in **1**, the spectra suggests a mononuclear vanadium(V) complex and it exhibits a singlet for each –OH and –HC=N in the region 10.34 and 9.39, ppm respectively [42]. The aromatic protons were observed in the expected range between δ = 8.59-6.77 ppm and additionally two sets of resonances that is, a quartet at δ = 3.08 and a triplet at 1.15 ppm were observed for N–CH$_2$- and –CH$_3$, respectively in the aliphatic region, which are attributed to the presence of a triethylammonium counterion [42]. In the case of **2** two equivalent sets of protons are observed which are attributed to dimerization of the complex through μ_2-oxido-bridging. The spectra exhibit singlets in the regions δ = 10.44-9.39 and 8.66 ppm for –OH and –HC=N, respectively. The aromatic protons were observed in the expected range between δ = 8.66-6.18 ppm [45]. The representative spectra of **1** (^{1}H, ^{13}C, and ^{51}V NMR) and **2** (^{1}H, and ^{51}V NMR) are depicted in the ESI section (Figures S3–S7).

2.2.4. ESI Mass Spectra

The mass spectral data for **1** and **2** were recorded in acetonitrile solution (Figures S8 and S9). The ESI mass spectra display characteristic molecular ion peaks at *m/z* 480.10 and 694.97 for **1** and **2**, respectively. In addition to the molecular ion peak, the complex **1** shows a peak at *m/z* 467.19 corresponding to the [M + H$^+$ + 0.5 H$_2$O]$^+$ aggregate.

2.3. Single-Crystal X-ray Crystallography of **1**

Crystals of salt **1** were obtained enabling a structure determination by X-ray crystallography. Salt **1** crystallizes in the triclinic space group P$^-$1 with two independent triethylammonium cations and two complex anions comprising the crystallographic asymmetric unit. The molecular structure of the first independent anion is shown in Figure 2a while those of the other constituents of the asymmetric unit are shown in Figure S10. Selected geometric parameters for the independent anions are listed in Table 1. The vanadium atom is penta-coordinated within a NO$_4$ donor set provided by an imine-N1, two phenoxide-O1, O2, and two oxido-O3, O4 atoms. The five-coordinate geometry is distorted from the ideal square-pyramidal and trigonal-bipyramidal geometries as quantified in

the values of τ [47]. For the ideal geometries, $\tau = 0.0$ and 1.0, respectively, whereas in the experimental structures τ computes to 0.26 (anion "a") and 0.24 (anion "b"). In this description, the V1 atom lies 0.4691(6) Å above the least-squares plane through the O1, O2, O4 and N1 atoms [r.m.s. deviation = 0.1663 Å] in the direction of the oxido-O3a atom; the comparable parameters for the V2-anion are 0.4935(6) and 0.0939 Å, respectively. The bond valency for the vanadium atoms, as calculated in PLATON [48], amount to 5.07 and 5.11, respectively, consistent with the assignment of vanadium(V) centers.
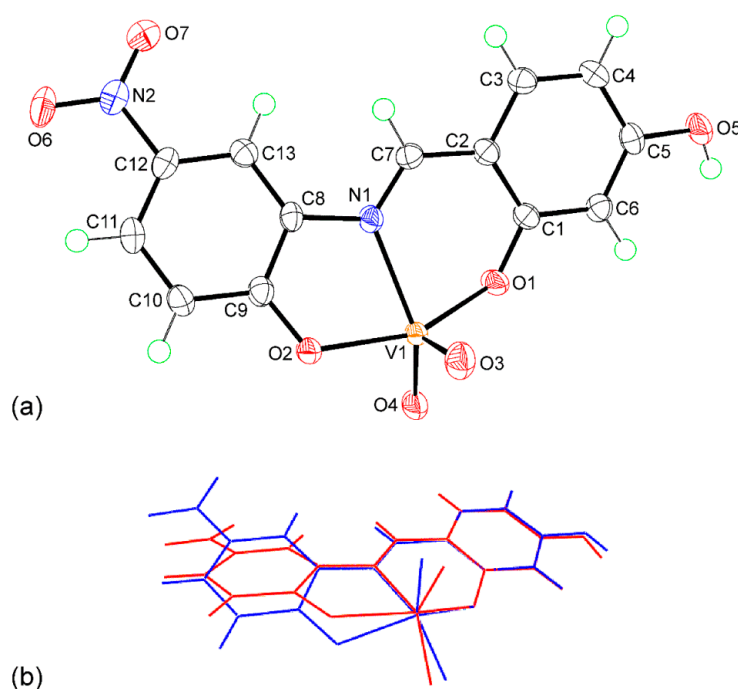

Figure 2. (**a**) Molecular structure of the first independent complex anion of salt **1** showing atom labelling scheme and displacement ellipsoids at the 70% probability level and (**b**) overlay diagram of the independent complex anions of **1**: red image, the molecule shown in (**a**). The molecule anions have been overlapped so the O1, C1, and C2 atoms are coincident.

Table 1. Selected geometric parameters (Å, °) for the independent anions in salt **1**.

Parameter	Anion "a"	Anion "b"
V–O1	1.9152(9)	1.8942(9)
V–O2	1.9735(9)	1.9191(9)
V–O3	1.6219(10)	1.6356(10)
V–O4	1.6463(9)	1.6473(10)
V–N1	2.1658(11)	2.1968(11)
C7–N1	1.3033(17)	1.2942(17)
O1–V–O2	155.41(4)	140.66(4)
O3–V–O4	109.05(5)	108.51(5)
N1–V–O4	140.02(5)	155.17(5)

The tridentate mode of coordination of the Schiff base dianion leads to the formation of six- and five-membered chelate rings. The best description of the six-membered ring is based on an envelope with the V1 atom being the flap atom. Here, the V1 atom lies 0.5624(15) Å out of the plane of the remaining atoms [r.m.s. deviation = 0.0348 Å]; the equivalent parameters for the second independent anion are 0.5256(15) and 0.0429 Å, respectively. By contrast, the five-membered ring for anion "a" is essentially planar exhibiting a r.m.s. deviation of 0.0239 Å with the maximum deviation of 0.0311(6) Å being for the N1a atom. However, an envelope conformation is the best description for the five-membered chelate ring of anion "b" whereby the V2 atom lies 0.5978(19) Å out of the

plane of the remaining four atoms [r.m.s. deviation of 0.0066 Å]. The conformational differences between the molecules are highlighted in the overlay diagram of Figure 2b. Some significant differences in geometric parameters are apparent, especially, the elongation of the V1–O2(phenoxide) bond length compared with the other comparable bonds, and the elongation of the V2–N1(imine) bond as well as differences of up to 15° in the O1–V–O2 and N1–V–O4 bond angles. Although these may relate to conformational disparities, the influence of hydrogen bonding interactions cannot be discounted.

The presence of hydroxyl-O–H · · · O(oxido) hydrogen bonds link the two independent anions into a two-molecule aggregate as shown in Figure 3; the geometric parameters characterizing the identified hydrogen bonding interactions in **1** are listed in Table 2. These hydrogen bonding interactions are consistent with the lengthening of the V–O4 bond lengths compared with the V–O3 bonds. Appended to the two-molecule aggregate are the triethylammonium cations which form charge-assisted N–H · · · O3 hydrogen bonds. The N3a-cation also forms a hydrogen bond to the O2 atom indicating the H1n atom is bifurcated; this interaction accounts, at least partially, for the lengthening of the V1–O2 bond (see above). As illustrated in Supplementary Figure S11, the four-molecule aggregates are assembled into a three-dimensional architecture featuring hydroxyphenyl-C–H · · · O(phenoxide), nitrophenyl-C–H · · · O(oxide, hydroxyl), methylene-C–H · · · O(phenoxide, oxide and nitro) and methyl-C–H · · · O(oxide) interactions, as detailed in Table S1.
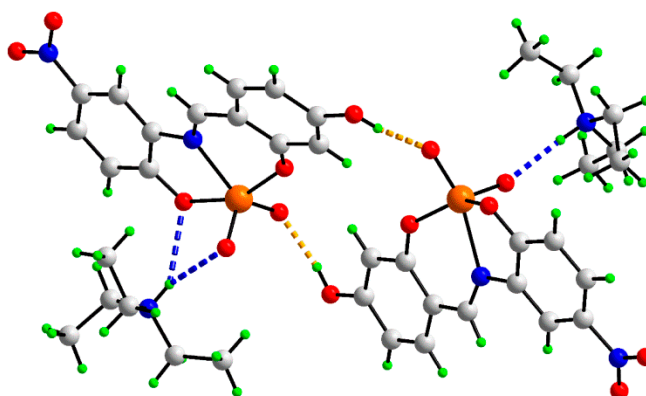

Figure 3. The four-molecule aggregate in **1** features hydroxyl-O–H · · · O(oxido) and charge-assisted N–H · · · O3 hydrogen bonds shown as orange and blue dashed lines, respectively.

Table 2. Geometric parameters (Å, °) characterizing the identified hydrogen bonding contacts between the constituents of the asymmetric unit of salt **1** leading to a four-molecule aggregate.

A	H	B	H···B	A···B	A–H···B
O5a	H1o	O4b	1.825(12)	2.6548(14)	171.3(18)
O5b	H2o	O4a	1.830(15)	2.6640(14)	171.7(17)
N3a	H1n	O2a	2.466(13)	3.2244(15)	145.4(13)
N3a	H1n	O3a	2.224(12)	2.9473(15)	139.8(14)
N3b	H2n	O3b	1.918(12)	2.7904(16)	170.7(14)

There are relatively few structural precedents for **1** in the crystallographic literature. Arguably the most closely related structure is that of [Et₃NH][VO₂L] where L is the 1-(((5-chloro-2-oxidophenyl)imino)methyl)naphthalen-2-olate dianion [11]. Here, a very similar square-pyramidal coordination geometry is noted with each chelate ring having an envelope conformation as seen for anion "b" in **1**.

2.4. DNA-Binding Studies

2.4.1. UV–Vis Absorption Studies

The interactions of metal complexes with DNA provide the binding information of metal complexes with the DNA helix [49]. Therefore, the absorption study was performed

by maintaining the concentration of the complexes constant (25 µM) with varying DNA concentrations from 0 to 100 µM. Upon increasing the CT–DNA concentration, hypochromic shifts are observed in both the complexes for the maximal peaks (Figure 4). Generally, hypochromism or hyperchromism shifts often are observed in the absorption spectrum of a metal complex when the complex interacts with DNA [50]. Hypochromism in absorption spectra is generally associated with the binding of complexes to DNA through the intercalation mode [51]. To compare the DNA-binding affinity of these compounds quantitatively, their intrinsic binding constants were calculated with the aid of the following equation: [52]

$$\frac{[DNA]}{\varepsilon_a - \varepsilon_f} = \frac{[DNA]}{\varepsilon_b - \varepsilon_f} + \frac{1}{K_b\left(\varepsilon_b - \varepsilon_f\right)} \tag{1}$$

where $[DNA]$ is the concentration of DNA base pairs, K_b is binding constant and ε_a, ε_f, and ε_b are the apparent extinction coefficients for the complex i.e., Abs/[complex] in the presence of DNA, in absence of DNA and fully bound of DNA, respectively. A plot of $[DNA]/(\varepsilon_a - \varepsilon_f)$ vs. $[DNA]$ gave a slope and an intercept equal to $1/(\varepsilon_b - \varepsilon_f)$ and $1/K_b(\varepsilon_b - \varepsilon_f)$, respectively, while the binding constant K_b was calculated from the ratio of the slope to the intercept. The intrinsic binding constants K_b were found to be 2.81×10^4 and 2.35×10^4 M^{-1} for **1** and **2**, respectively (Table 3). From the binding constant values, it is clear that complex **1** interacts more strongly with CT−DNA. However, the free ligand H$_2$L itself shows good binding activity (1.59×10^4 M^{-1}) with DNA molecules [53,54].
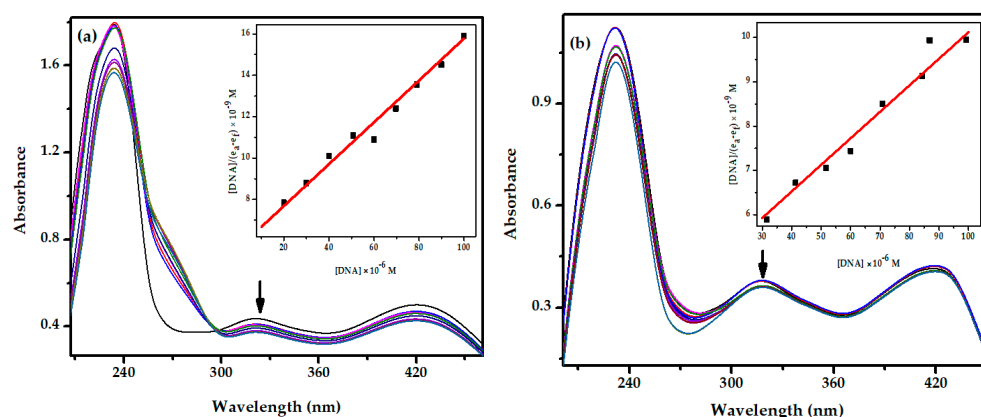

Figure 4. Absorption spectroscopic study of complex **1** (**a**) and **2** (**b**) (25 µM) with increasing concentrations of CT–DNA (0–100 µM). The inset shows the plots of $[DNA]/(\varepsilon_a - \varepsilon_f)$ versus $[DNA]$ for the titration of the prepared compounds with CT–DNA.

Table 3. DNA-binding parameters for **1**, **2**, and H$_2$L.

Complex	Binding Constants (K_b) (M^{-1})
1	2.81×10^4
2	2.35×10^4
H$_2$L	1.59×10^4

2.4.2. Circular Dichroism Studies

Circular dichroism (CD) studies were performed to investigate the conformational changes in CT–DNA upon interaction with the new compounds. The spectra show two significant CD bands in the UV region, a positive band at 275 nm due to base stacking whereas a negative band at 245 nm is due to right handed helicity [38,51]. In intercalation mode of small molecules, there occurs perturbation in the spectra whereas for groove binding and electrostatic interaction there will be minimal or no perturbation [38,51]. However, from Figure 5, it is observed that there are significant changes in the CD spectra

of CT–DNA which further suggest that the tested compounds bind to CT–DNA in an intercalating mode.
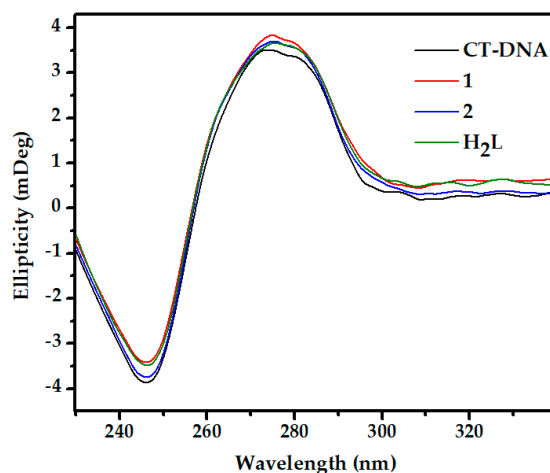

Figure 5. Circular dichroism spectra of CT–DNA (150 µM) in the presence and absence H_2L, and complexes (**1** and **2**) in 50 mM Tris–HCl buffer (pH 7.4). The path length of the cuvette was 5 mm.

2.5. Cytotoxicity

According to GLOBOCAN 2020, disease occurrence and mortality due to colorectal cancer has increased to 1.9 million. Moreover, it has been placed as the third most and second most incidences in terms of mortality in both male and female, respectively. Furthermore, the incidence of colorectal cancer has been reported to be the most in eastern Asian countries such as India. Therefore, in this study we have chosen a most aggressive colorectal cancer cell line HT-29 [55]. Hence, the cytotoxicity of the oxidovandium(V) complexes (**1** and **2**) were measured against HT-29 cancer and NIH-3T3 normal cells by MTT assay and were compared to the ligand (H_2L) alone. The IC_{50} values are listed in Table 4, and the cell viability percentage diagrams are depicted in Figure 6. Specifically, the cytotoxicity of **1** and **2** exhibited IC_{50} values 8.56 ± 0.62, and 9.09 ± 0.03 µM, respectively, while that of the ligand alone was determined to be 7.75 ± 0.53 µM against HT-29 cancer cell line. These findings suggest that with respect to the ligand, the coordination to vanadium did not improve its activity; in fact, H_2L is marginally more active than both of the complexes. As mentioned earlier, the polyphenol groups in ligand molecule (H_2L) induce apoptosis in cancer cells which is the primary reason towards the enhanced toxicity [28,53].

Furthermore, the cytotoxicity of the tested complexes was studied against the normal cell line NIH-3T3. The NIH-3T3 cell line is one of the most frequently used cell lines as the results provided by these tests can easily be compared with data published in the literature [56,57]. The results indicated there was a decrease in the cell viability upon the same exposure of the compounds. This result indicates that tested complexes were less damaging towards NIH-3T3 as compared to cancer cell lines. Additionally, it was observed that the ligand precursor H_2L is more selective against HT-29 cells than both complex molecules with selectivity index (SI) = 8.94, whereas SI values for **1** and **2** are 7.92 and 8.77, respectively. On the other hand, under the same experimental conditions the tested compounds exhibited comparable cytotoxicity against HT-29 compared with commonly used chemotherapeutic drugs such as cisplatin [58]. Furthermore, the results obtained on the present study may be also compared with previously reported oxidovanadium(V) complexes of Schiff base ligands such as [VO(sal-L-tryp)(Me-ATSC)], [VO(sal-Ltryp)(N-ethhymethohcarbthio)]·H_2O) and, [VO(sal-L-tryp)(acetylethTSC)]·C_2H_5OH with $IC_{50} > 47$ µM against HT-29 cell lines [59]. Additionally, we can also compare our results with recent work where two oxido-bridged vanadium(V) complexes of Schiff base ligands [{V^VO(R-salval)(H_2O)}(μ_2-O){V^VO(R-salval)}] and [{V^VO(R-vanval)(CH_3OH)}$_2$(μ_2-O)] (val = valine, sal = salicylaldehyde, and van = o-vanillin)

were investigated for cytotoxic studies against human hepatoma cell line with IC_{50} values > 200 μM [7].

Table 4. IC_{50} values of H_2L and Complexes (**1** and **2**) taking 10, 50, and 100 μM concentrations.

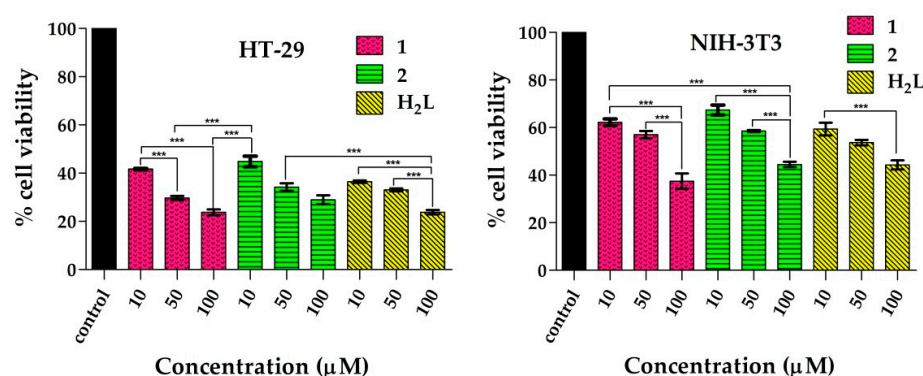| Compound	IC_{50} (μM)	
	HT-29	**NIH-3T3**
1	8.56 ± 0.62	67.85 ± 5.48
2	9.09 ± 0.03	79.77 ± 4.00
H_2L	7.75 ± 0.53	69.32 ± 4.42

Figure 6. The effect of **1**, **2**, and H_2L on the cell viability of HT-29 and NIH-3T3 cells after 48 h of exposure, taking 10, 50, and 100 μM concentrations of the compounds. The cell viability was calculated by MTT assay. Data were reported as the mean ± SD for n = 4. *** *p* < 0.0001 was considered statistically significant.

2.6. Nuclear DAPI Staining Assay

To examine the apoptotic potential of test compounds in HT-29 cells, DAPI staining assay was conducted. Chromatin condensation, cell shrinkage, and nuclear fragmentation during the process of apoptosis (type I programmed cell death) is a distinguishing marker of nuclear change [51]. For this assay HT-29 cells were treated with 20 μM of H_2L, **1** and **2**, respectively and then the cells were incubated for 24 h before DAPI nuclear staining. Later, the image of cells was captured under fluorescent microscope fitted with a DAPI filter. The nuclear blebbings and brightly condensed chromatin bodies were marked by arrows in Figure 7.
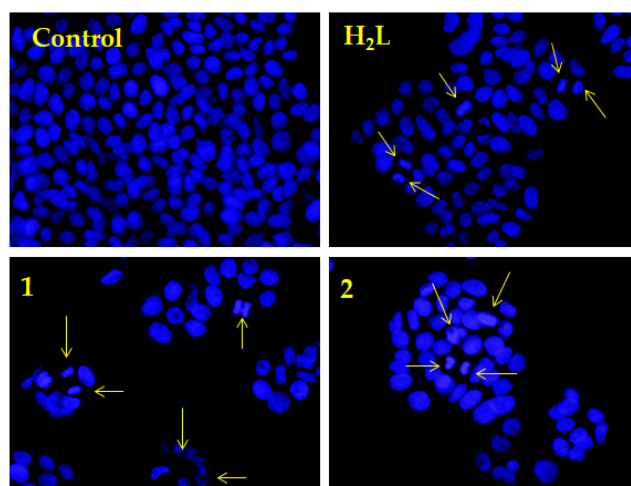

Figure 7. Study of apoptosis by morphological changes in nuclei of HT-29 cells. Arrows show the morphological changes in the nuclei of HT-29 cells observed on applying H_2L, **1**, and **2** in comparisons to control.

3. Materials and Methods

3.1. Materials

All the starting materials such as 2-amino-4-nitrophenol, and 2,4-dihydroxybenzaldehyde were purchased from Sigma Aldrich and used without further purification. Reagent grade solvents were dried and distilled prior to use. [VO(acac)$_2$] was prepared by the reported method [60]. MTT (3-[4, 5-dimethylthiazol-2-yl]-2, 5-diphenyltetrazolium), DAPI (4', 6-diamidino-2-phenylindoledihydrochloride), and CT–DNA were purchased from Sigma Aldrich (St. Louis, MO, USA). HT-29 and NIH-3T3 cell lines were procured from National Centre for Cell Science (NCCS), Pune, India. CHN analyses were carried out on a Vario ELcube CHNS Elemental analyzer. ESI–MS data of the complexes were recorded on a Waters XEVO G2-XS QTOF MS instrument operating in positive ion mode. IR spectra were recorded on a Perkin-Elmer Spectrum RXI spectrophotometer. ^{1}H and ^{13}C NMR spectra were recorded on a Bruker Ultrashield 400 MHz spectrometer in the presence of SiMe$_4$ as the internal standard. Electronic spectra were recorded on a Shimadzu spectrophotometer (UV-2450).

3.2. Synthesis of Ligands

The Schiff base ligand H$_2$L was synthesized by refluxing 2,4-dihydroxy-benzaldehyde and 2-amino-4-nitrophenol in equimolar ratio in ethanol following a standard procedure [13]. The resulting compound was isolated through filtration, washed with ethanol, and dried over fused CaCl$_2$ under desiccator conditions. The molecular structure of the compound was confirmed by elemental and spectroscopic (FT-IR, UV–Vis, and NMR (^{1}H, ^{13}C{^{1}H})) analysis.

H$_2$L: Yield: 67%. Anal. calcd. for C$_{13}$H$_{10}$N$_2$O$_5$ (274.23): C, 56.94; H, 3.68; N, 10.22. Found: C, 56.81; H, 3.61; N, 10.18. IR (KBr pellet, cm^{-1}): 3205 ν(O–H); 1632 ν(C=N). UV–Vis (DMSO) [λ$_{max}$, nm (ε, M^{-1} cm^{-1})]: 317 (6817), 278 (6812). ^{1}H NMR (400 MHz, DMSO-d$_6$): δ (ppm) = 10.92 (s, 1H, –OH), 10.35 (s, 2H, –OH), 9.25 (s, 1H, –OH), 8.95 (s, 2H, –OH), 8.21 (s, 2H, HC=N–), 8.20–6.27 (m, 12H, aromatic). ^{13}C{^{1}H} NMR (100 MHz, DMSO-d$_6$): δ (ppm) = 191.51, 167.47, 165.67, 165.39, 163.71, 162.04, 156.52, 153.69, 140.32, 140.19, 137.87, 133.30, 131.57, 130.21, 124.65, 118.13, 116.72, 115.64, 115.53, 114.73, 112.83, 110.52, 110.16, 109.11, 103.01, 102.67.

3.3. Synthesis of Oxidovanadium(V) Complexes

(HNEt$_3$)[V^{V}O$_2$L] (**1**). This was synthesized by refluxing the H$_2$L (0.27 g, 1 mmol) and VO(acac)$_2$ (0.265 g, 1 mmol) in hot absolute ethanol (20 mL) using triethylamine as a base for 4 h. Dark brown crystals were obtained from the filtrate after 2–4 days. The crystals were filtered and washed with ethanol for X-ray structure determination. (HNEt$_3$)[V^{V}O$_2$L] (**1**): Yield: 0.32 g (70%). Anal. calcd. for C$_{19}$H$_{24}$N$_3$O$_7$V (457.35): C, 49.90; H, 5.29; N, 9.19; found C, 49.87; H, 5.22; N, 9.12. IR (KBr pellet, cm^{-1}): 2986 ν(O–H), 1607 ν(C=N), 947, 890 ν(V=O). UV–Vis (DMSO) [λ$_{max}$, nm (ε, M^{-1} cm^{-1})]: 428 (6242), 317 (4331), 265 (4356). ^{1}H NMR (400 MHz, DMSO-d$_6$): δ (ppm) = 10.34 (s, 1H,–OH), 9.39 (s, 1H, HC=N–), 8.59–6.17 (m, 6H, aromatic), 3.09 (m, 6H, N-CH$_2$), 1.17 (m, 9H, –CH$_3$). ^{13}C{^{1}H} NMR (100 MHz, DMSO-d$_6$): δ (ppm) = 169.41, 165.60, 159.26, 136.92, 136.81, 136.33, 133.50, 125.03, 124.63, 116.14, 115.22, 114.86, 111.05, 46.26, 9.31. ^{51}V NMR (DMSO-d$_6$): δ (ppm) = −527.86. ESI–MS: *m/z* 480.1007 [M + Na]$^+$.

[(V^{V}OL)$_2$μ-O] (**2**). This complex was synthesized by refluxing the H$_2$L (0.27 g, 1 mmol) and VO(acac)$_2$ (0.265 g, 1 mmol) in hot MeCN (20 mL) for 4 h. Dark brown crystalline materials were obtained from the filtrate after 2–4 days. The crystalline materials were filtered and washed with ethanol. [(V^{V}OL)$_2$μ-O] (**2**): Yield: 0.45 g (66%). Anal. calcd. for C$_{26}$H$_{16}$N$_4$O$_{13}$V$_2$ (694.30): C, 44.98; H, 2.32; N, 8.07; found C, 44.92; H, 2.22; N, 8.13. IR (KBr pellet, cm−1): 2986 ν(O–H), 1607 ν(C=N), 975, 891 ν(V=O). UV–Vis (DMSO) [λ$_{max}$, nm (ε, M^{-1} cm^{-1})]: 446 (6037), 361 (1956), 264 (2450). ^{1}H NMR (400 MHz, DMSO-d$_6$): δ (ppm) = 10.44 (s, 1H, –OH), 8.63 (s, 2H, –OH), 8.01–6.18 (m, 12H, aromatic). ^{13}C{^{1}H} NMR (100 MHz, DMSO-d$_6$): δ (ppm) = 168.18, 163.71, 159.21, 156.82, 143.28, 141.33, 131.72, 121.78,

118.32, 117.56, 111.07, 108.71, 102.88. ^{51}V NMR (DMSO-d_6): δ (ppm) = −575.27, −530.96. ESI–MS: *m/z* 694.9722 [M + H]$^+$.

3.4. Single-Crystal X-ray Crystallography

X-ray Intensity data for a brown crystal of **1** (0.06 × 0.19 × 0.24 mm) were measured at 100 K on Rigaku/Oxford Diffraction XtaLAB Synergy diffractometer (Dualflex, AtlasS2) fitted with CuKα radiation (α = 1.54178 Å) so that θ_{max} = 67.1° (= 100% completeness). Data reduction, including Gaussian absorption correction, was accomplished with CrysAlisPro [61]. The structure was solved by direct-methods [62] and refined (anisotropic displacement parameters and H atoms in the riding model approximation) on F^2 [63]. The O- and N-bound H atoms were located from Fourier difference maps and refined with distance constraints of O–H = 0.84 ± 01 Å and N–H = 0.88 ± 01 Å, respectively. A weighting scheme of the form w = 1/[$\sigma^2(F_o^2)$ + (0.043P)^2 + 0.792P], where P = (F_o^2 + 2F_c^2)/3, was introduced towards the end of the refinement. The molecular structure diagrams were generated with ORTEP for Windows [64] with 70% displacement ellipsoids, and the packing diagrams were drawn with DIAMOND [65]. Crystal data and refinement details are given in Table 5.

Table 5. Crystallographic data and refinement details for salt **1**.

Formula	[C$_6$H$_{16}$N][C$_{13}$H$_8$N$_2$O$_7$V]
Molecular weight	457.35
Crystal system	triclinic
Space group	$P\bar{1}$
a/Å	10.8226(1)
b/Å	10.9399(2)
c/Å	17.3389(3)
α/°	79.412(1)
β/°	78.905(1)
γ/°	86.861(1)
V/Å^3	1979.82(5)
Z	4
D_c/g cm^{-3}	1.534
μ/mm^{-1}	4.621
Measured data	46,958
Unique data	7061
Observed data ($I \geq 2.0\sigma(I)$)	6958
No. parameters	559
R, obs. data; all data	0.025; 0.026
R_w, obs. data; all data	0.072; 0.072
Range of residual electron density peaks/eÅ^{-3}	−0.58–0.23

3.5. DNA-Binding Experiments

3.5.1. UV–Vis Absorption Studies

The interaction of the ligand and its respective oxidovanadium(V) complexes (**1** and **2**) with CT–DNA was investigated by the absorption titration method with a Shimadzu spectrophotometer (UV–2450) [39,40,42,51]. The absorption titration of DNA was conducted by using a fixed concentration of metal complex (25 μM) in 50 mM Tris–HCl buffer (pH = 7.4), with gradual increases in concentration of the CT–DNA from 0 to 100 μM. Each of the above experiments was performed in triplicate at room temperature and the incubation time was 5 min after the subsequent addition of CT–DNA for each time to equilibrate DNA and the complexes properly.

3.5.2. Circular Dichroism Studies

Circular dichroism study was performed in a JASCO J-1500 CD Spectrophotometer at 25 °C using a quartz cell with 5 mm path length [51]. CD spectra of CT–DNA (150 μM)

were collected both in the presence and absence of complexes (25 μM) at a wavelength range of 230–350 nm in 50 mM Tris–HCl buffer (pH 7.4) (HiMedia), after averaging three accumulations and a scan speed of 200 nm/min.

3.6. Cytotoxicity Analysis through MTT Assay

The cytotoxicity of the ligand molecule and its respective vanadium(V) complexes was evaluated against colon cancer (HT-29) and mouse embryonic fibroblast (NIH-3T3) cells using the MTT (3-[4, 5-dimethylthiazol-2-yl]-2, 5-diphenyltetrazolium) assay [42]. All cell lines were cultured in DMEM (Dulbecco's phosphate-buffered saline) medium supplemented with 10% FBS (Fetal bovine serum) and maintained at 37 °C in a CO_2 incubator (5% CO_2) and humidified atmosphere (95% humidity). During the MTT assays, cells were seeded in 96-well plates at a density of 6×10^3 cells per well after cell counting in a hemocytometer and allowed for 70–80% confluence. Then complexes and the ligand were dissolved in DMSO at a concentration of 100 mM and suitably diluted in DMEM media to achieve final working concentrations of 10, 50, and 100 μM. After 12 h of initial seeding, the HT-29 and NIH-3T3 cells were treated with the above prepared concentrations of each complex and further subjected to incubation for 48 h. MTT was dissolved in the DPBS (Dulbecco's Modified Eagle Medium) solution and was added to the culture medium. After additional 3 h incubation at 37 °C, the media were carefully removed and 200 μL of DMSO was added to each well and the absorbance values were determined by spectrophotometry at 595 nm with a microplate reader spectrophotometer (Perkin-Elmer 2030). The results were expressed as percentages of the control.

% cell viability = [mean OD of the treated cell/mean OD of the control] × 100

IC_{50} value of the compounds was calculated from the absorbance concentration plot following standard procedure [51,66].

3.7. Nuclear DAPI Staining Assay

The morphology of nucleus during the cell death of cells in response to treatment with the complexes was investigated using fluorescence microscopy (Olympus IX 71). DAPI (4′, 6-diamidino-2-phenylindoledihydrochloride) stain was used for this nuclear staining assay and was performed according to a standard procedure previously reported [67]. Accordingly, HT-29 cells were treated with treated (20 μM of compound for 24 h) and untreated cells were fixed with 4% paraformaldehyde for 15 min. Then the cells were stained with DAPI and incubated for 5 min at 37 °C after washing two times with DPBS. Finally, again after washing with DPBS, the cells were examined by fluorescence microscopy.

4. Conclusions

In this work, two new oxidovanadium(V) complexes $(HNEt_3)[V^VO_2L]$ (**1**), and $[(V^VOL)_2\mu\text{-}O]$ (**2**) have been synthesized using a Schiff base ligand (H_2L) derived from 2,4-dihydroxybenzaldehyde and 2-amino-4-nitrophenol. The ligand and complexes were characterized by FT-IR, UV–Vis, and NMR (^{1}H, ^{13}C, and [51]V) spectroscopy, ESI–MS, and the purity was confirmed by CHN analysis. The molecular structure of **1** was determined by X-ray crystallography indicating a distorted square-pyramidal geometry for the vanadium(V) center defined by imine-N, two phenoxide-O, and two oxido-O atoms. DNA-binding experiments were conducted using a UV–Vis absorption titration method and circular dichroism studies and the results suggested that the ligand as well as the complexes have considerable DNA-binding propensity. From the results, complex **1**, displayed maximum DNA-binding activity with $K_b = 2.81 \times 10^4$ M^{-1}. From circular dichroism studies it was further confirmed that the synthesized molecules interacted with DNA through the intercalation mode. Finally, from the results of cytotoxicity studies it is confirmed that all the tested compounds including the ligand molecule induce cell death against HT-29 cells mainly through the apoptotic mode. However, the ligand molecule with $IC_{50} = 7.75 \pm 0.53$ μM was found more cytotoxic than its corresponding complexes.

In addition, the cytotoxicity of ligand and complexes was also studied against NIH-3T3 normal cells, and it was found to be relatively less damaging towards them. In summary, the present group of compounds should stimulate further in vitro and in vivo studies of related compounds as part of the quest to develop new drugs for the treatment of cancer.

Supplementary Materials: The following are available online at https://www.mdpi.com/article/10.3390/inorganics9090066/s1, Figure S1: IR spectra of H$_2$L and **1**, Figure S2: ^{1}H NMR spectra of H$_2$L, Figure S3-S5: ^{1}H, ^{13}C, and ^{51}V of **1**, Figure S6-S7: ^{1}H and ^{51}V NMR spectra of **2**, Figure S8-S9: ESI–MS of **1** and **2**, Figure S10: independent molecular structure of cation and anion of **1**, Figure S11. A view of the unit-cell contents for salt **1**, Table S1: Geometric parameters (Å, °) of **1**.

Author Contributions: R.D.: Conceptualization, Visualization, Supervision, Funding acquisition. G.S.: Investigation, Validation, Writing-original draft, review, and editing. E.R.T.T.: Investigation, Writing-original draft, review, and editing. All authors have read and agreed to the published version of the manuscript.

Institutional Review Board Statement: Not applicable.

Informed Consent Statement: Not applicable.

Data Availability Statement: Not applicable.

Conflicts of Interest: The authors declare no conflict of interest.

References

1. Pessoa, J.C.; Garribba, E.; Santos, M.F.A.; Santos-Silva, T. Vanadium and proteins: Uptake, transport, structure, activity and function. *Coord. Chem. Rev.* **2015**, *301–302*, 49–86. [CrossRef]
2. Rehder, D. The future of/for vanadium. *Dalton Trans.* **2013**, *42*, 11749–11761. [CrossRef]
3. Thompson, K. Coordination chemistry of vanadium in metallopharmaceutical candidate compounds. *Coord. Chem. Rev.* **2001**, *219–221*, 1033–1053. [CrossRef]
4. Baran, E.J. Oxovanadium(IV) and oxovanadium(V) complexes relevant to biological systems. *J. Inorg. Biochem.* **2000**, *80*, 1–10. [CrossRef]
5. Domingues, N.; Pelletier, J.; Ostenson, C.-G.; Castro, M.M.C.A. Therapeutic properties of VO(dmpp)$_2$ as assessed by in vitro and in vivo studies in type 2 diabetic GK rats. *J. Inorg. Biochem.* **2014**, *131*, 115–122. [CrossRef]
6. Pillai, S.I.; Subramanian, S.P.; Kandaswamy, M. A novel insulin mimetic vanadium-flavonol complex: Synthesis, characterization and in vivo evaluation in STZ-induced rats. *Eur. J. Med. Chem.* **2013**, *63*, 109–117. [CrossRef] [PubMed]
7. Turtoi, M.; Anghelache, M.; Patrascu, A.A.; Maxim, C.; Manduteanu, I.; Calin, M.; Popescu, D.-L. Synthesis, Characterization, and In Vitro Insulin-Mimetic Activity Evaluation of Valine Schiff Base Coordination Compounds of Oxidovanadium(V). *Biomedicines* **2021**, *9*, 562. [CrossRef] [PubMed]
8. Dash, S.P.; Pasayat, S.; Bhakat, S.; Roy, S.; Dinda, R.; Tiekink, E.R.T.; Mukhopadhyay, S.; Bhutia, S.K.; Hardikar, M.R.; Joshi, B.N.; et al. Highly stable hexacoordinated nonoxidovanadium(IV) complexes of sterically constrained ligands: Syntheses, structure, and study of antiproliferative and insulin mimetic activity. *Inorg. Chem.* **2013**, *52*, 14096–14107. [CrossRef] [PubMed]
9. Orvig, C.; Caravan, P.; Gelmini, L.; Glover, N.; Herring, F.G.; Li, H.; McNeill, J.H.; Rettig, S.J.; Setyawati, I.A. Reaction chemistry of BMOV, bis(maltolato)oxovanadium(IV), a potent insulin mimetic agent. *J. Am. Chem. Soc.* **1995**, *117*, 12759–12770. [CrossRef]
10. Evangelou, A.M. Vanadium in cancer treatment. *Crit. Rev. Oncol.* **2002**, *42*, 249–265. [CrossRef]
11. Ebrahimipour, S.Y.; Sheikhshoaie, I.; Kautz, A.C.; Ameri, M.; Pasban-Aliabadi, H.; Amiri Rudbari, H.; Bruno, G.; Janiak, C. Mono- and dioxido-vanadium(V) complexes of a tridentate ONO Schiff base ligand: Synthesis, spectral characterization, X-ray crystal structure, and anticancer activity. *Polyhedron* **2015**, *93*, 99–105. [CrossRef]
12. Levina, A.; Pires Vieira, A.; Wijetunga, A.; Kaur, R.; Koehn, J.T.; Crans, D.C.; Lay, P.A. A Short-Lived but Highly Cytotoxic Vanadium(V) Complex as a Potential Drug Lead for Brain Cancer Treatment by Intratumoral Injections. *Angew. Chem. Int. Ed. Engl.* **2020**, *59*, 15834–15838. [CrossRef]
13. Banerjee, A.; Dash, S.P.; Mohanty, M.; Sahu, G.; Sciortino, G.; Garribba, E.; Carvalho, M.F.N.N.; Marques, F.; Costa Pessoa, J.; Kaminsky, W.; et al. New V^{IV}, V^{IV}O, V^{V}O, and V^{V}O$_2$ Systems: Exploring their Interconversion in Solution, Protein Interactions, and Cytotoxicity. *Inorg. Chem.* **2020**, *59*, 14042–14057. [CrossRef]
14. Bishayee, A.; Waghray, A.; Patel, M.A.; Chatterjee, M. Vanadium in the detection, prevention and treatment of cancer: The in vivo evidence. *Cancer Lett.* **2010**, *294*, 1–12. [CrossRef]

15. Ni, L.; Zhao, H.; Tao, L.; Li, X.; Zhou, Z.; Sun, Y.; Chen, C.; Wei, D.; Liu, Y.; Diao, G. Synthesis, in vitro cytotoxicity, and structure-activity relationships (SAR) of multidentate oxidovanadium(IV) complexes as anticancer agents. *Dalton Trans.* **2018**, *47*, 10035–10045. [CrossRef] [PubMed]

16. Sutradhar, M.; Pombeiro, A.J.L. Coordination chemistry of non-oxido, oxido and dioxidovanadium(IV/V) complexes with azine fragment ligands. *Coord. Chem. Rev.* **2014**, *265*, 89–124. [CrossRef]

17. Rezaeivala, M.; Keypour, H. Schiff base and non-Schiff base macrocyclic ligands and complexes incorporating the pyridine moiety—The first 50 years. *Coord. Chem. Rev.* **2014**, *280*, 203–253. [CrossRef]

18. Gupta, K.C.; Sutar, A.K. Catalytic activities of Schiff base transition metal complexes. *Coord. Chem. Rev.* **2008**, *252*, 1420–1450. [CrossRef]

19. Liu, X.; Hamon, J.-R. Recent developments in penta-, hexa- and heptadentate Schiff base ligands and their metal complexes. *Coord. Chem. Rev.* **2019**, *389*, 94–118. [CrossRef]

20. Khan, M.I.; Khan, A.; Hussain, I.; Khan, M.A.; Gul, S.; Iqbal, M.; Inayat-Ur-Rahman; Khuda, F. Spectral, XRD, SEM and biological properties of new mononuclear Schiff base transition metal complexes. *Inorg. Chem. Commun.* **2013**, *35*, 104–109. [CrossRef]

21. Zhang, N.; Fan, Y.-h.; Zhang, Z.; Zuo, J.; Zhang, P.-f.; Wang, Q.; Liu, S.-B.; Bi, C.-F. Syntheses, crystal structures and anticancer activities of three novel transition metal complexes with Schiff base derived from 2-acetylpyridine and l-tryptophan. *Inorg. Chem. Commun.* **2012**, *22*, 68–72. [CrossRef]

22. Tsuchida, E. Oxovanadium(III–V) mononuclear complexes and their linear assemblies bearing tetradentate Schiff base ligands: Structure and reactivity as multielectron redox catalysts. *Coord. Chem. Rev.* **2003**, *237*, 213–228. [CrossRef]

23. Patra, S.; Chatterjee, S.; Si, T.K.; Mukherjea, K.K. Synthesis, structural characterization, VHPO mimicking peroxidative bromination and DNA nuclease activity of oxovanadium(V) complexes. *Dalton Trans.* **2013**, *42*, 13425–13435. [CrossRef]

24. Sathyadevi, P.; Krishnamoorthy, P.; Butorac, R.R.; Cowley, A.H.; Bhuvanesh, N.S.P.; Dharmaraj, N. Effect of substitution and planarity of the ligand on DNA/BSA interaction, free radical scavenging and cytotoxicity of diamagnetic Ni(II) complexes: A systematic investigation. *Dalton Trans.* **2011**, *40*, 9690–9702. [CrossRef]

25. Raj Kumar, R.; Mohamed Subarkhan, M.K.; Ramesh, R. Synthesis and structure of nickel(II) thiocarboxamide complexes: Effect of ligand substitutions on DNA/protein binding, antioxidant and cytotoxicity. *RSC Adv.* **2015**, *5*, 46760–46773. [CrossRef]

26. Galati, G.; Chan, T.; Wu, B.; O'Brien, P.J. Glutathione-dependent generation of reactive oxygen species by the peroxidase-catalyzed redox cycling of flavonoids. *Chem. Res. Toxicol.* **1999**, *12*, 521–525. [CrossRef]

27. Galati, G. Prooxidant activity and cellular effects of the phenoxyl radicals of dietary flavonoids and other polyphenolics. *Toxicology* **2002**, *177*, 91–104. [CrossRef]

28. Rice-Evans, C.A.; Miller, N.J.; Paganga, G. Structure-antioxidant activity relationships of flavonoids and phenolic acids. *Free Radic. Biol. Med.* **1996**, *20*, 933–956. [CrossRef]

29. Prior, R.L.; Wu, X.; Gu, L. Flavonoid metabolism and challenges to understanding mechanisms of health effects. *J. Sci. Food Agric.* **2006**, *86*, 2487–2491. [CrossRef]

30. Kessler, M.; Ubeaud, G.; Jung, L. Anti- and pro-oxidant activity of rutin and quercetin derivatives. *J. Pharm. Pharmacol.* **2003**, *55*, 131–142. [CrossRef]

31. Pasayat, S.; Böhme, M.; Dhaka, S.; Dash, S.P.; Majumder, S.; Maurya, M.R.; Plass, W.; Kaminsky, W.; Dinda, R. Synthesis, Theoretical Study and Catalytic Application of Oxidometal (Mo or V) Complexes: Unexpected Coordination Due to Ligand Rearrangement through Metal-Mediated C-C Bond Formation. *Eur. J. Inorg. Chem.* **2016**, *2016*, 1604–1618. [CrossRef]

32. Dinda, R.; Majhi, P.K.; Sengupta, P.; Pasayat, S.; Ghosh, S.; Falvello, L.R.; Mak, T.C.W. Alkali metal (Na$^+$ and K$^+$)-mediated supramolecular assembly of oxovanadium(V) complexes: Synthesis and structural characterization. *Polyhedron* **2010**, *29*, 248–253. [CrossRef]

33. Dash, S.P.; Pasayat, S.; Saswati; Dash, H.R.; Das, S.; Butcher, R.J.; Dinda, R. Oxovanadium(V) complexes incorporating tridentate aroylhydrazoneoximes: Synthesis, characterizations and antibacterial activity. *Polyhedron* **2012**, *31*, 524–529. [CrossRef]

34. Dash, S.P.; Panda, A.K.; Dhaka, S.; Pasayat, S.; Biswas, A.; Maurya, M.R.; Majhi, P.K.; Crochet, A.; Dinda, R. A study of DNA/BSA interaction and catalytic potential of oxidovanadium(V) complexes with ONO donor ligands. *Dalton Trans.* **2016**, *45*, 18292–18307. [CrossRef]

35. Saswati; Adão, P.; Majumder, S.; Dash, S.P.; Roy, S.; Kuznetsov, M.L.; Pessoa, J.C.; Gomes, C.S.B.; Hardikar, M.R.; Tiekink, E.R.T.; et al. Synthesis, structure, solution behavior, reactivity and biological evaluation of oxidovanadium(IV/V) thiosemicarbazone complexes. *Dalton Trans.* **2018**, *47*, 11358–11374. [CrossRef]

36. Banerjee, A.; Dash, S.P.; Mohanty, M.; Sanna, D.; Sciortino, G.; Ugone, V.; Garribba, E.; Reuter, H.; Kaminsky, W.; Dinda, R. Chemistry of mixed-ligand oxidovanadium(IV) complexes of aroylhydrazones incorporating quinoline derivatives: Study of solution behavior, theoretical evaluation and protein/DNA interaction. *J. Inorg. Biochem.* **2019**, *199*, 110786. [CrossRef]

37. Roy, S.; Böhme, M.; Dash, S.P.; Mohanty, M.; Buchholz, A.; Plass, W.; Majumder, S.; Kulanthaivel, S.; Banerjee, I.; Reuter, H.; et al. Anionic Dinuclear Oxidovanadium(IV) Complexes with Azo Functionalized Tridentate Ligands and μ-Ethoxido Bridge Leading to an Unsymmetric Twisted Arrangement: Synthesis, X-ray Structure, Magnetic Properties, and Cytotoxicity. *Inorg. Chem.* **2018**, *57*, 5767–5781. [CrossRef]

38. Dash, S.P.; Panda, A.K.; Pasayat, S.; Dinda, R.; Biswas, A.; Tiekink, E.R.T.; Mukhopadhyay, S.; Bhutia, S.K.; Kaminsky, W.; Sinn, E. Oxidovanadium(V) complexes of aroylhydrazones incorporating heterocycles: Synthesis, characterization and study of DNA binding, photo-induced DNA cleavage and cytotoxic activities. *RSC Adv.* **2015**, *5*, 51852–51867. [CrossRef]

39. Lima, S.; Banerjee, A.; Mohanty, M.; Sahu, G.; Kausar, C.; Patra, S.K.; Garribba, E.; Kaminsky, W.; Dinda, R. Synthesis, structure and biological evaluation of mixed ligand oxidovanadium(IV) complexes incorporating 2-(arylazo)phenolates. *New J. Chem.* **2019**, *43*, 17711–17725. [CrossRef]

40. Banerjee, A.; Mohanty, M.; Lima, S.; Samanta, R.; Garribba, E.; Sasamori, T.; Dinda, R. Synthesis, structure and characterization of new dithiocarbazate-based mixed ligand oxidovanadium(IV) complexes: DNA/HSA interaction, cytotoxic activity and DFT studies. *New J. Chem.* **2020**, *44*, 10946–10963. [CrossRef]

41. Dash, S.P.; Panda, A.K.; Pasayat, S.; Majumder, S.; Biswas, A.; Kaminsky, W.; Mukhopadhyay, S.; Bhutia, S.K.; Dinda, R. Evaluation of the cell cytotoxicity and DNA/BSA binding and cleavage activity of some dioxidovanadium(V) complexes containing aroylhydrazones. *J. Inorg. Biochem.* **2015**, *144*, 1–12. [CrossRef]

42. Mohanty, M.; Maurya, S.K.; Banerjee, A.; Patra, S.A.; Maurya, M.R.; Crochet, A.; Brzezinski, K.; Dinda, R. In vitro cytotoxicity and catalytic evaluation of dioxidovanadium(V) complexes in an azohydrazone ligand environment. *New J. Chem.* **2019**, *43*, 17680–17695. [CrossRef]

43. Dash, S.P.; Panda, A.K.; Pasayat, S.; Dinda, R.; Biswas, A.; Tiekink, E.R.T.; Patil, Y.P.; Nethaji, M.; Kaminsky, W.; Mukhopadhyay, S.; et al. Syntheses and structural investigation of some alkali metal ion-mediated $LV^VO_2^-$ (L^{2-} = tridentate ONO ligands) species: DNA binding, photo-induced DNA cleavage and cytotoxic activities. *Dalton Trans.* **2014**, *43*, 10139–10156. [CrossRef] [PubMed]

44. Dash, S.P.; Roy, S.; Mohanty, M.; Carvalho, M.F.N.N.; Kuznetsov, M.L.; Pessoa, J.C.; Kumar, A.; Patil, Y.P.; Crochet, A.; Dinda, R. Versatile Reactivity and Theoretical Evaluation of Mono- and Dinuclear Oxidovanadium(V) Compounds of Aroylazines: Electrogeneration of Mixed-Valence Divanadium(IV,V) Complexes. *Inorg. Chem.* **2016**, *55*, 8407–8421. [CrossRef]

45. Dash, S.P.; Majumder, S.; Banerjee, A.; Carvalho, M.F.N.N.; Adão, P.; Pessoa, J.C.; Brzezinski, K.; Garribba, E.; Reuter, H.; Dinda, R. Chemistry of Monomeric and Dinuclear Non-Oxido Vanadium(IV) and Oxidovanadium(V) Aroylazine Complexes: Exploring Solution Behavior. *Inorg. Chem.* **2016**, *55*, 1165–1182. [CrossRef] [PubMed]

46. Nemeikaite-Ceniene, A.; Imbrasaite, A.; Sergediene, E.; Cenas, N. Quantitative structure-activity relationships in prooxidant cytotoxicity of polyphenols: Role of potential of phenoxyl radical/phenol redox couple. *Arch. Biochem. Biophys.* **2005**, *441*, 182–190. [CrossRef]

47. Addison, A.W.; Rao, T.N.; Reedijk, J.; van Rijn, J.; Verschoor, G.C. Synthesis, structure, and spectroscopic properties of copper(II) compounds containing nitrogen–sulphur donor ligands; the crystal and molecular structure of aqua[1,7-bis(*N*-methylbenzimidazol-2′-yl)-2,6-dithiaheptane]copper(II) perchlorate. *J. Chem. Soc. Dalton Trans.* **1984**, 1349–1356. [CrossRef]

48. Spek, A.L. checkCIF validation ALERTS: What they mean and how to respond. *Acta Crystallogr. E Crystallogr. Commun.* **2020**, *76*, 1–11. [CrossRef]

49. Krishnamoorthy, P.; Sathyadevi, P.; Butorac, R.R.; Cowley, A.H.; Bhuvanesh, N.S.P.; Dharmaraj, N. Copper(I) and nickel(II) complexes with 1:1 vs. 1:2 coordination of ferrocenyl hydrazone ligands: Do the geometry and composition of complexes affect DNA binding/cleavage, protein binding, antioxidant and cytotoxic activities? *Dalton Trans.* **2012**, *41*, 4423–4436. [CrossRef] [PubMed]

50. Sirajuddin, M.; Ali, S.; Badshah, A. Drug-DNA interactions and their study by UV-Visible, fluorescence spectroscopies and cyclic voltammetry. *J. Photochem. Photobiol. B* **2013**, *124*, 1–19. [CrossRef] [PubMed]

51. Saswati; Mohanty, M.; Banerjee, A.; Biswal, S.; Horn, A.; Schenk, G.; Brzezinski, K.; Sinn, E.; Reuter, H.; Dinda, R. Polynuclear zinc(II) complexes of thiosemicarbazone: Synthesis, X-ray structure and biological evaluation. *J. Inorg. Biochem.* **2020**, *203*, 110908. [CrossRef] [PubMed]

52. Ganeshpandian, M.; Loganathan, R.; Suresh, E.; Riyasdeen, A.; Akbarsha, M.A.; Palaniandavar, M. New ruthenium(II) arene complexes of anthracenyl-appended diazacycloalkanes: Effect of ligand intercalation and hydrophobicity on DNA and protein binding and cleavage and cytotoxicity. *Dalton Trans.* **2014**, *43*, 1203–1219. [CrossRef]

53. Tan, J.; Wang, B.; Zhu, L. DNA binding and oxidative DNA damage induced by a quercetin copper(II) complex: Potential mechanism of its antitumor properties. *J. Biol. Inorg. Chem.* **2009**, *14*, 727–739. [CrossRef]

54. Perron, N.R.; Hodges, J.N.; Jenkins, M.; Brumaghim, J.L. Predicting how polyphenol antioxidants prevent DNA damage by binding to iron. *Inorg. Chem.* **2008**, *47*, 6153–6161. [CrossRef]

55. Sung, H.; Ferlay, J.; Siegel, R.L.; Laversanne, M.; Soerjomataram, I.; Jemal, A.; Bray, F. Global Cancer Statistics 2020: GLOBOCAN Estimates of Incidence and Mortality Worldwide for 36 Cancers in 185 Countries. *CA Cancer J. Clin.* **2021**, *71*, 209–249. [CrossRef]

56. Krishnamoorthy, P.; Sathyadevi, P.; Cowley, A.H.; Butorac, R.R.; Dharmaraj, N. Evaluation of DNA binding, DNA cleavage, protein binding and in vitro cytotoxic activities of bivalent transition metal hydrazone complexes. *Eur. J. Med. Chem.* **2011**, *46*, 3376–3387. [CrossRef]

57. Raja, D.S.; Paramaguru, G.; Bhuvanesh, N.S.P.; Reibenspies, J.H.; Renganathan, R.; Natarajan, K. Effect of terminal *N*-substitution in 2-oxo-1,2-dihydroquinoline-3-carbaldehyde thiosemicarbazones on the mode of coordination, structure, interaction with protein, radical scavenging and cytotoxic activity of copper(II) complexes. *Dalton Trans.* **2011**, *40*, 4548–4559. [CrossRef]

58. Chen, Y.; Qin, M.-Y.; Wu, J.-H.; Wang, L.; Chao, H.; Ji, L.-N.; Xu, A.-L. Synthesis, characterization, and anticancer activity of ruthenium(II)-β-carboline complex. *Eur. J. Med. Chem.* **2013**, *70*, 120–129. [CrossRef]

59. Mohamadi, M.; Yousef Ebrahimipour, S.; Torkzadeh-Mahani, M.; Foro, S.; Akbari, A. A mononuclear diketone-based oxido-vanadium(V) complex: Structure, DNA and BSA binding, molecular docking and anticancer activities against MCF-7, HPG-2, and HT-29 cell lines. *RSC Adv.* **2015**, *5*, 101063–101075. [CrossRef]

60. Moeller, T. (Ed.) *Inorganic Syntheses*; Mc-Graw Hill Book Company: New York, NY, USA, 1957; Volume 5, pp. 113–116.

61. Rigaku Oxford Diffraction. *CrysAlisPRO*; Rigaku Oxford Diffraction Ltd.: Oxfordshire, UK, 2017.
62. Sheldrick, G.M. A short history of SHELX. *Acta Crystallogr. A* **2008**, *64*, 112–122. [CrossRef]
63. Sheldrick, G.M. Crystal structure refinement with SHELXL. *Acta Crystallogr. C Struct. Chem.* **2015**, *71*, 3–8. [CrossRef]
64. Farrugia, L.J. WinGX and ORTEP for Windows: An update. *J. Appl. Crystallogr.* **2012**, *45*, 849–854. [CrossRef]
65. Brandenburg, K.; Berndt, M. *DIAMOND, Version 3.2k*; GbR: Bonn, Germany, 2006.
66. Roy, S.; Mohanty, M.; Miller, R.G.; Patra, S.A.; Lima, S.; Banerjee, A.; Metzler-Nolte, N.; Sinn, E.; Kaminsky, W.; Dinda, R. Probing CO Generation through Metal-Assisted Alcohol Dehydrogenation in Metal-2-(arylazo)phenol Complexes Using Isotopic Labeling (Metal = Ru, Ir): Synthesis, Characterization, and Cytotoxicity Studies. *Inorg. Chem.* **2020**, *59*, 15526–15540. [CrossRef]
67. Bhutia, S.K.; Mallick, S.K.; Maiti, S.; Maiti, T.K. Antitumor and proapoptotic effect of Abrus agglutinin derived peptide in Dalton's lymphoma tumor model. *Chem. Biol. Interact.* **2008**, *174*, 11–18. [CrossRef]